OCEANOGRAPHY

10.1126/sciadv.1600282

Anticyclonic eddies are more productive than cyclonic eddies in subtropical gyres because of winter mixing

François Dufois,[1]* Nick J. Hardman-Mountford,[1]* Jim Greenwood,[1] Anthony J. Richardson,[2,3] Ming Feng,[1] Richard J. Matear[4]

Mesoscale eddies are ubiquitous features of ocean circulation that modulate the supply of nutrients to the upper sunlit ocean, influencing the rates of carbon fixation and export. The popular eddy-pumping paradigm implies that nutrient fluxes are enhanced in cyclonic eddies because of upwelling inside the eddy, leading to higher phytoplankton production. We show that this view does not hold for a substantial portion of eddies within oceanic subtropical gyres, the largest ecosystems in the ocean. Using space-based measurements and a global biogeochemical model, we demonstrate that during winter when subtropical eddies are most productive, there is increased chlorophyll in anticyclones compared with cyclones in all subtropical gyres (by 3.6 to 16.7% for the five basins). The model suggests that this is a consequence of the modulation of winter mixing by eddies. These results establish a new paradigm for anticyclonic eddies in subtropical gyres and could have important implications for the biological carbon pump and the global carbon cycle.

INTRODUCTION

Subtropical ocean gyres represent the most extensive ecosystems in the world, covering ~40% of Earth's surface (*1*). Although their biological productivity per unit area is small, they are major contributors to biogeochemical cycles, especially carbon cycling, because of their large size (*1*, *3*). Their biological productivity is limited by the weak vertical nutrient supply to the euphotic zone (*1*, *2*) and is predicted to be further reduced under future climate change because of a decrease in vertical mixing (*4*). However, this large scale mean picture is modulated by mesoscale eddies, which contribute to horizontal and vertical nutrient fluxes into the euphotic zone (*5*, *6*).

Observations in the North Atlantic and North Pacific during the 1990s led to the popular "eddy pumping" hypothesis, which describes the upward doming of isopycnal surfaces accompanied by an enhanced vertical nutrient supply and elevated productivity in cyclonic eddies (CEs) (*7*). The eddy pumping paradigm has since been challenged several times; nonetheless, environments in which anticyclonic eddies (ACEs) have elevated chlorophyll (CHL) were thought to be unusual, unique, or contrasting (*8*–*10*). Although eddy pumping is still considered a major process in open ocean eddies (*11*), the most recent literature retains that oceanic productivity is modulated by eddies through a range of processes (*5*, *12*–*14*), some of which even enhances productivity in ACEs (*13*, *15*). Both eddy induced mixing and eddy induced Ekman pumping are likely to enhance nutrient fluxes into the euphotic zone in ACEs, but assessing the relative contribution of these processes has proved difficult (*5*, *10*, *15*). Here, we challenge the eddy pumping paradigm at the global scale and show that ACEs are more productive than CEs in all five subtropical gyres because of modulation of winter convective mixing.

[1]Commonwealth Scientific and Industrial Research Organisation, Oceans and Atmosphere, Private Bag 5, Wembley, Western Australia 6913, Australia. [2]Commonwealth Scientific and Industrial Research Organisation, Oceans and Atmosphere, Ecosciences Precinct, Brisbane, Queensland 4102, Australia. [3]Centre for Applications in Natural Resource Mathematics, School of Mathematics and Physics, University of Queensland, St Lucia, Queensland 4072, Australia. [4]Commonwealth Scientific and Industrial Research Organisation, Oceans and Atmosphere, GPO Box 1538, Hobart, Tasmania 7001, Australia.
*Corresponding author. Email: fdufois@gmail.com (F.D.); Nick.Hardman Mountford@csiro.au (N.J.H. M.)

RESULTS AND DISCUSSION

Eddy/CHL relationship

To analyze the relationship between eddies and surface CHL, we averaged SeaWiFS (Sea Viewing Wide Field of View Sensor) CHL within the interior of each eddy obtained from the database of Chelton *et al.* (*16*), which was derived from satellite measured sea surface height. Using a weekly database of 97,541 ACEs and 106,068 CEs over 13 years across oligotrophic subtropical gyres, our analyses show that surface CHL peaks during winter in both ACEs and CEs (Fig. 1, C to G). During winter, and in contrast to the eddy pumping theory, surface CHL within ACEs is generally higher than that within CEs in areas of low surface CHL and deep nutricline (Fig. 1A). This effect is greatest in the Indian Ocean but is present in all subtropical gyres, representing a large fraction of the total ocean area (Fig. 1B). In the South Indian Ocean gyre, the mean surface CHL is higher in ACEs than in CEs by 16.7 ± 0.9% (table S1) and by more than 28% for 10% of the gyre area (table S2). The effect is smaller but still persistent in the South Pacific and South Atlantic gyres, with mean surface CHL being higher by 7.4 ± 0.7% and 6.2 ± 1.0%, respectively, in ACEs than in CEs. The effect is smallest but still apparent in the North Atlantic and North Pacific, with an increase of 4.8 ± 0.8% and 3.6 ± 0.7%, respectively (table S1).

Eddy/CHL variability

To interpret the eddy/CHL relationship in the subtropics, we performed Rotated Empirical Orthogonal Function (REOF) analysis over patterns of normalized CHL anomaly in ACEs during winter. It shows three main modes of variability, each explaining 31.8, 16.2, and 9.5% of the total variance (Fig. 2A). Whereas the first two modes are consistent with stirring of background CHL by eddies (*12*) (see the

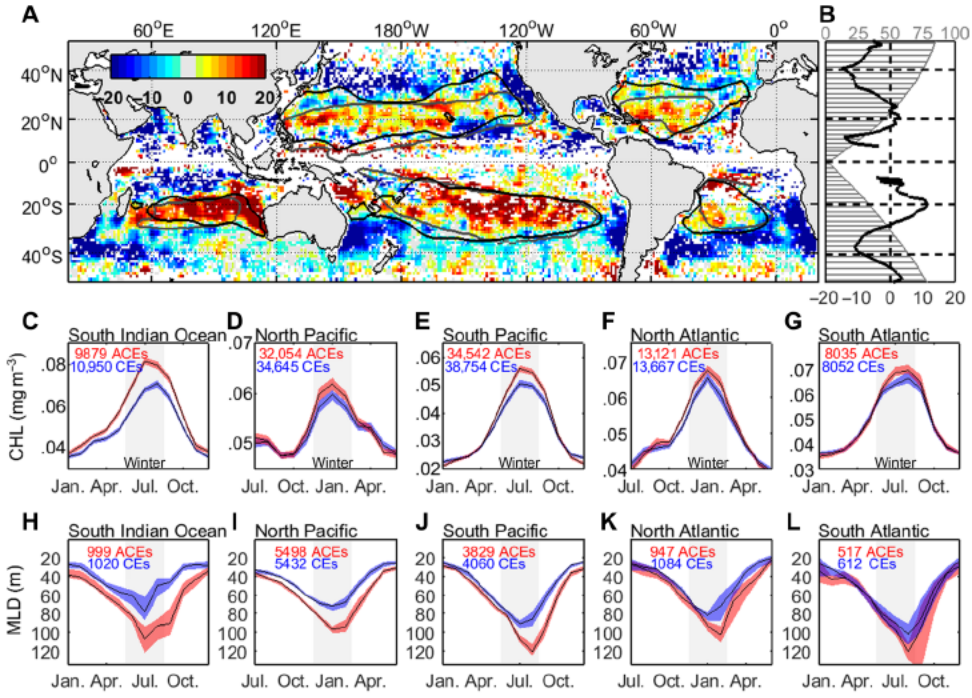

Fig. 1. Surface CHL and MLD difference between ACE and CE interiors ($r/R \leq 1$). (**A**) Relative difference R_d (%) between ACEs and CEs during winter (December to February, northern hemisphere; June to August, southern hemisphere). Gray contours highlight the maximum seasonal CHL concentration of 0.1 mg m^{-3}. Black contours denote where the maximum winter nutricline depth is 110-m deep. R_d is computed over a 1° resolution grid, and noise is removed by applying a 5° running mean (refer to fig. S1 before the running mean is applied). The number of eddies used to produce the map is shown in fig. S2. (**B**) Latitudinal average of R_d (%) (black) and cumulative fraction of ocean area (%) for each hemisphere starting from the equator (gray). (**C** to **L**) Seasonal median values and associated 95% confidence intervals of CHL (C to G) and Argo-derived MLD (H to L) in ACEs (black lines, red shading) and CEs (black lines, blue shading) in the five subtropical gyres.

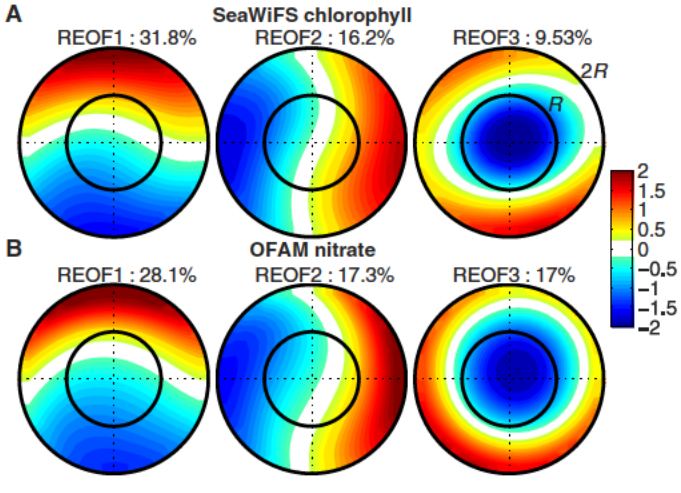

Fig. 2. REOF decomposition of the normalized anomaly of satellite CHL and modeled NO_3 in winter ACEs from 50°S to 50°N. (**A** and **B**) First three REOF spatial patterns for satellite surface CHL (A) and modeled surface nitrate (B). The fraction of the variance explained by the REOF is indicated above each pattern. Inner and outer circles coincide with $r/R = 1$ (eddy perimeter) and $r/R = 2$.

Supplementary Materials), the third mode highlights mesoscale processes in their center. This third mode corresponds to either a positive or a negative CHL anomaly in the eddy center, depending on the sign of the principal component. Positive CHL anomalies in ACE centers related to the third REOF mode are found primarily in subtropical gyres (Fig. 3A). The REOF analysis for CEs provides similar results, showing that CEs with negative anomalies in their centers are mostly found in subtropical gyres (figs. S3A and S4A). Furthermore, the third REOF mode for ACEs is the only mode that can increase CHL in eddy centers at the scale of subtropical gyres (fig. S5). Although not all eddies in the subtropical gyres exhibit this "anomalous" behavior (~31% on average) (Fig. 3A and fig. S4A), very few (~6%) exhibit the eddy pumping behavior (Fig. 3B and fig. S4B).

NO_3 modeling

To identify potential processes responsible for this higher surface CHL in ACEs, we used the global biogeochemical model of Ocean Forecasting Australia Model (OFAM). REOF modes obtained for the modeled surface NO_3 within ACEs are strikingly similar to the SeaWiFS CHL REOF modes (Fig. 2B). The third mode of variability, accounting for 17.0% of the variance, highlights a clear modulation of surface nitrate in ACE centers, and positive nitrate anomalies in ACEs are mostly found in subtropical gyres (Fig. 3C). The REOF analysis for

CEs is also consistent with the SeaWiFS CHL analysis in terms of patterns, although the ordering of the main modes differs (figs. S3B and S4, C and D).

Eddy processes

REOF analyses of both the model and the observations suggest that the differences in Fig. 1A are nutrient driven and originate from meso scale processes within eddy centers. It is unlikely that eddy stirring, mostly acting along the edge and captured in the first two REOF modes, is responsible. Furthermore, the OFAM did not include eddy wind interactions (that is, surface currents do not affect wind friction) (*17*). Therefore, in our model at least, the increased nitrate modeled at the surface of ACEs during winter is not related to eddy induced Ekman pumping (*13*) a mechanism previously suggested to explain increased nitrate fluxes into the euphotic zone in ACEs in the South Indian Ocean (*10*).

Instead, the modulation of winter convective mixing by eddies, an alternative mechanism proposed for the South Indian Ocean (*15*), is responsible, at least partly, for modulating the seasonal input of nitrate in eddies within the five subtropical gyres. Summer stratification is weaker in ACEs than in CEs (Fig. 4), allowing winter convective mixing to reach deeper and resulting in deeper mixed layer depths (MLD) in ACEs (Fig. 1, H to L), which are consistent with expecta tions (*15*, *18*). This results in ACEs having an enriched nitrate concen tration just below the MLD, which allows greater injection of nitrate into the mixed layer (Fig. 5). The model shows that deeper mixing in ACE centers during winter enhances nutrient fluxes (fig. S6A) and can supply the surface increase in nitrate (fig. S6B). The mean picture from a statistical approach (Fig. 5) is consistent with the model for individual eddies, although smaller scale processes coexist (fig. S7).

Eddy driven processes often occur out of satellite view, at the base of the euphotic zone. Therefore, the satellite analysis itself, highlighting an increase in CHL at the near surface layer of ACEs, does not nec essarily provide a complete picture of eddy induced changes in CHL or the associated biological productivity. However, vertical nitrate fluxes into the mixed layer are enhanced in ACEs in the model, suggesting that the productivity could be increased in the mixed layer.

Eddy pumping and eddy-induced mixing

In temperate latitudes, eastern boundary upwelling systems, and west ern boundary currents, CEs have greater surface CHL than ACEs (Figs. 1A and 3B and fig. S4B). This could be due to eddy pumping and other processes producing the same results. In temperate re gions that are light limited rather than nutrient limited, phyto plankton in ACEs are mixed deeper and thus experience lower average light levels (*5*, *19*), producing negative CHL anomalies. The light replete but oligotrophic central parts of the subtropical gyres contrast with that of the conceptual model because they rely more on vertical mixing to bring nutrients to the euphotic zone (*20*). The eddy pumping mechanism still operates in subtropical gyres during winter but only affects the nitrate field at depth, whereas it is over whelmed by eddy induced mixing within surface layers (Fig. 5).

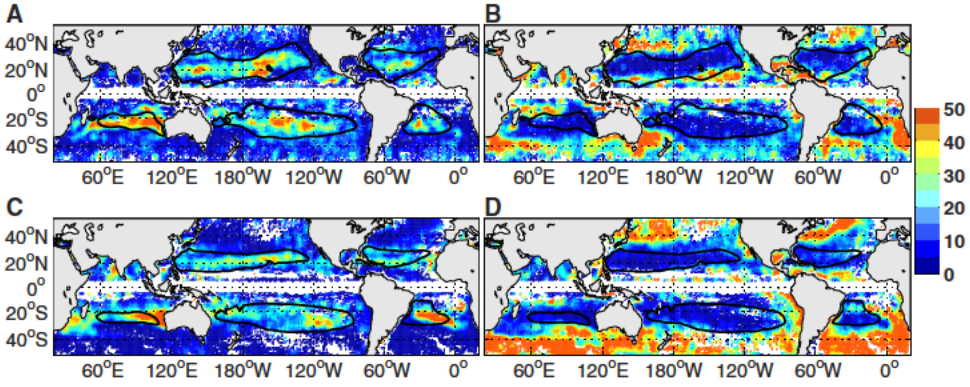

Fig. 3. Spatial distribution of CHL and NO_3 anomaly localized within the perimeter of ACEs during winter on the basis of the third principal component of their REOF decomposition (see Fig. 2). (**A** to **D**) The proportion of ACEs (%) with loadings less than −1 SD [(A) for CHL, (C) for NO_3; that is, strong positive anomaly] and greater than 1 SD [(B) for CHL, (D) for NO_3; that is, strong negative anomaly]. Values are computed over a 1° resolution grid, and noise is removed by applying a 5° running mean. Black contours denote where the maximum winter nutricline depth is 110-m deep.

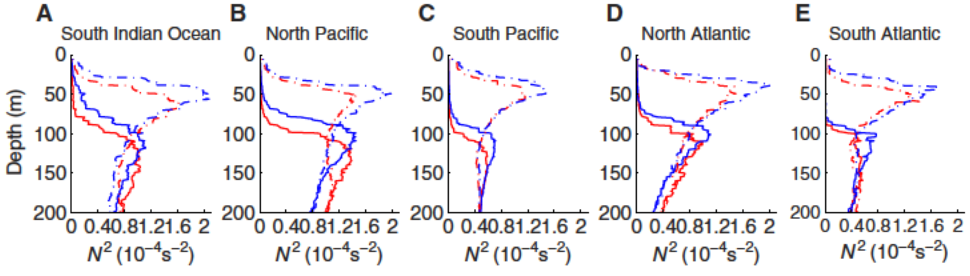

Fig. 4. Eddy stratification in the five subtropical gyres. (**A** to **E**) Median squared buoyancy frequency N^2 from Argo floats in ACEs (red) and CEs (blue) during summer (dotted lines) and during winter (solid lines).

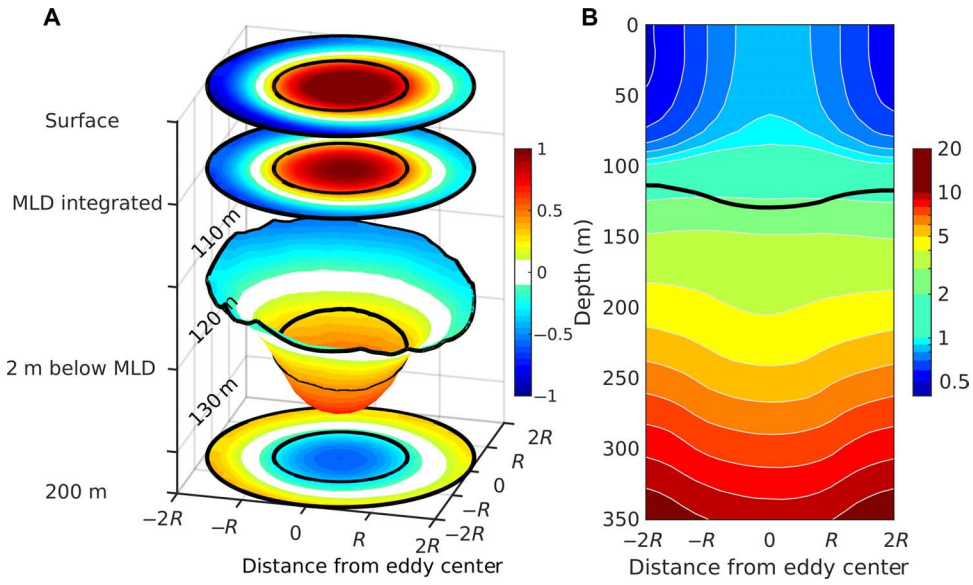

Fig. 5. Median vertical structure of modeled NO_3 for all winter ACEs where the third principal component (Fig. 2B) is lower than −1 SD. (**A**) NO_3 anomaly composite at the surface, integrated within the MLD, 2 m below the MLD, and at a 200-m depth. Inner and outer circles coincide with $r/R = 1$ (eddy perimeter) and $r/R = 2$. (**B**) Median NO_3 (mmol m^{-3}) along a longitudinal section crossing the eddy centers. The black line corresponds to the median MLD.

CONCLUSIONS

Downwelling eddies in subtropical gyres can no longer be considered barren deserts but as equally or more productive than their upwell ing counterparts. The summer stratification is weaker in ACEs than in CEs, and allows for deeper mixing during winter, but without the light limitation of higher latitudes. Subtropical gyres may account for half of the global ocean organic carbon pump (*3*) and play a role in mitigating global warming (*21*, *22*), especially if anthropogenic climate forcing enhances eddy activity (*23*). However, the impact of eddy related nutrient budgets (*7*, *24* *26*) on primary production under climate change (*4*, *23*) should be revisited in the subtropical gyres to account for convective mixing as a key mesoscale process supplying nutrients to the euphotic zone. This should be underpinned by high resolution biogeochemical sampling in ACEs during winter to better understand how the productivity in ACEs influences the biological pump (*21*, *26*).

MATERIALS AND METHODS

Data

Our analysis was based on eight daily SeaWiFS satellite observations of oceanic CHL at a 9 km resolution from September 1997 to December 2010 (available at http://oceancolor gsfc.nasa gov/). To fill gaps in the CHL data set due to cloud cover, we applied a temporal low pass filter, removing variability shorter than a month. CHL data were also smoothed using a spatial 1° × 1° low pass filter.

We used the eddy database of Chelton *et al.* (*16*) from October 1992 to January 2011. For each eddy over the SeaWiFS period, we colocated the CHL field in space and time. The distance from eddy center r was normalized by the eddy radius R (that is, the location of strongest geostrophic current), and the associated CHL field was projected into the normalized "eddy frame" (that is, for each individual eddy, CHL values at distance r were projected to r/R). Furthermore, for a comparison of northern and southern hemisphere eddies, the lower end of the eddy frame corresponded to the equatorward side of the eddy (that is, north and south were flipped for southern hemisphere eddies).

Over a 1° × 1° resolution grid, we computed the relative CHL difference R_d (%) between ACEs and CEs in eddy centers ($r/R \leq 1$) using the equation

$$R_d = \frac{\overline{\mathrm{CHL}}(\mathrm{ACEs}) - \overline{\mathrm{CHL}}(\mathrm{CEs})}{\overline{\mathrm{CHL}}} \quad (1)$$

where $\overline{\mathrm{CHL}}$ denotes the median of CHL.

We used temperature and salinity profiles from Argo floats (down loaded from www.argo.net) that coincided with the eddy database period. After colocating the Argo floats with eddies, we only retained the floats inside eddy centers ($r/R \leq 1$). The MLD was computed from the Argo temperature profiles. The base of the mixed layer corresponded to the depth where the temperature changes by 0.2°C, compared to the temperature at a 10 m depth. We also computed the squared buoyancy (Brunt Väisälä) frequency N^2 using the formula $N^2 = -g/\rho_0 \frac{\partial \rho}{\partial z}$, where ρ is the potential density calculated from temperature and salinity, g is the gravitational acceleration, and the reference density $\rho_0 = 1025$ kg m^{-3}. N^2 is commonly used to assess water column stratification (for example, the buoyancy production term of turbulent kinetic energy in vertical turbu lent closure models relies on N^2). Finally, we computed the median cli matology of both MLD and N^2 in both ACEs and CEs. We also used the National Oceanic and Atmospheric Administration World Ocean Atlas 2009 nitrate climatology data (available at www.nodc noaa gov).

Model

We used the OFAM eddy resolving biogeochemical model spanning the period 1993 2010 (*17*). It is a three dimensional NPZD (nitrate

phytoplankton zooplankton detritus) model with 1/10° horizontal resolution, developed to hindcast and forecast upper ocean conditions in nonpolar regions. OFAM uses the vertical mixing scheme described by Chen *et al.* (*27*). The model simulates nitrate supply to the photic zone; however, there is a delay when this nitrate is consumed by phytoplankton because the phytoplankton are light limited at the time of MLD maximum. This model behavior, which reflects the parameter values for phytoplankton growth and grazing, causes the seasonal maximum in phytoplankton to occur later in the season when light levels start to increase. Because simulated seasonal evolution of phytoplankton is out of phase with the observations, we used the simulated nitrate field to show how MLD deepening increases nitrate levels. Because the simulated annual mean nitrate value has spatial biases, we used spatially normalized nitrate anomalies to assess the nitrate spatial variability. Using the weekly sea surface height outputs, we tracked the eddies in the model using the algorithm proposed by Halo *et al.* (*28*), combining geometric and Okubo Weiss methods (available at www.simocean.org.za). Similar to the CHL data, for each eddy in the model, the NO_3 field was colocated and projected into the normalized eddy frame.

Anomalies

For each variable V (either satellite CHL or modeled NO_3), normalized anomalies V' were computed for each individual eddy as

$$V' = \frac{V - \overline{V}}{\sigma(V - \overline{V})} \tag{2}$$

where $\overline{V} = \frac{1}{4\pi R^2}\int_0^{2\pi}\int_0^{2R} V\, r\, dr\, d\theta$ is the mean V and σ is the SD, which are both computed over the eddy for $r \leq 2R$.

EOF analysis

We performed EOF analysis to decompose the patterns of normalized surface CHL and NO_3 anomalies within eddies. The analysis was performed using eddies between 50°S and 50°N. Eddies close to the equator (between 5°S and 5°N) were removed from this analysis. A rotation of the EOF (REOF) was performed using a varimax transformation, including the first three EOF modes. EOF rotation is commonly used in atmospheric sciences and oceanography to obtain physically interpretable patterns. The idea of the varimax rotation is to simplify the EOF patterns by tending the principal components toward 0 or large values. Thus, it is easier to identify each variable (that is, in our case, each eddy CHL pattern) with a single REOF spatial pattern. The varimax rotation is orthogonal, and the uncorrelatedness of the REOF patterns is preserved. Here, the rotation allowed for better comparisons between the SeaWiFS CHL modes and the OFAM nitrate modes than the simple EOF decomposition did. We only retained the first three modes of variability. The subsequent EOF spatial patterns were consistently spatially meaningless and represented less than 6% of the total variance. Furthermore, REOF spatial patterns were scaled (multiplied) by the maximum absolute value of the principal component with the sign of the mean principal component. The principal components therefore lay between −1 and 1, and the positive expression of the REOF modes corresponded to the most common one.

REOF analysis identifies patterns, but they are not fixed and can vary between a positive and a negative expression (principal components can oscillate in sign). To identify which REOF expression dominates regionally, we computed the proportion of each principal component to be outside ±1 SD for each 1° × 1° grid point. The 1 SD cutoff was chosen to only select for eddies with a strong loading on the considered REOF spatial pattern. Because this cutoff value is arbitrary, we tested other values and 0 in particular. Although the absolute proportion obviously differs when changing the cutoff value, it is interesting to note that the regional patterns highlighting the dominance of one or the other expression remain consistent (Fig. 3 and fig. S8).

Mixed layer nitrate budget

We computed the rate of change in nitrate within the mixed layer using the following equation (*15*)

$$\frac{\partial \bar{C}}{\partial t} = \varphi + \text{residual with } \varphi = -\frac{1}{h}\left\{(\bar{C} - C_{-h})\frac{\partial h}{\partial t}\right\} \tag{3}$$

where h is the MLD, C is the nitrate concentration, C_{-h} is the nitrate concentration at the base of the mixed layer, and $\bar{C}$ is the vertical average of C over the mixed layer (that is, $\bar{C} = \frac{1}{h}\int_{-h}^{0} C dz$). In this equation, φ is the rate of change in nitrate within the mixed layer induced by the change in MLD.

The nitrate budget was computed 2 m below the MLD using median climatological values. To separate the impacts of the different modes of variability on the nitrate budget, we calculated the nitrate rates of change for both positive and negative expressions of each EOF mode, selecting eddies whose principal component values are below or above 1 SD at least once in their life span. The time integrated nitrate rate of change starting in summer (July in the north hemisphere and January in the south hemisphere) was computed using $\Phi = \int_t \varphi dt$. We then compared Φ_{in} and Φ_{out}, the time integrated nitrate rate of change inside ($r/R \leq 1$) and outside ($1 < r/R \leq 2$) eddy centers, with $\overline{NO_3}_{in}$ and $\overline{NO_3}_{out}$, the mixed layer average nitrate concentration inside and outside eddies.

Subtropical gyre boundaries

Here, we considered the oligotrophic subtropical gyres as the subtropical areas with low CHL (<0.1 mg m^{-3}) and deep nutricline (>110 m). For each of the five subtropical gyres, all analyses were computed for the area inside both gray and black contours in Fig. 1A. Gray contours highlight the maximum seasonal CHL concentration of 0.1 mg m^{-3}, whereas black contours denote where the maximum winter nutricline depth is 110 m deep. The nutricline depth is the depth at which nitrate concentration exceeds 1 mmol m^{-3}.

SEs and confidence intervals

The SE was computed as SE = $\sigma/\sqrt{n}$, where σ is the SD and n is the size of the sample. We computed the 95% confidence interval for the median using actual values from the sample. The lower and upper 95% confidence limits were given by the ranked values $\frac{n}{2} - \frac{1.96\sqrt{n}}{2}$ and $1 + \frac{n}{2} + \frac{1.96\sqrt{n}}{2}$.

SUPPLEMENTARY MATERIALS

Supplementary material for this article is available at http://advances.sciencemag.org/cgi/content/full/2/5/e1600282/DC1

Comparison between the results obtained by Chelton *et al.* (*12*) and the REOF analysis

fig. S1. Same as Fig. 1, with no spatial smoothing (running mean) of R_d.
fig. S2. Spatial distribution of eddies.
fig. S3. REOF decomposition of the normalized anomaly of satellite CHL and modeled NO_3 in winter CEs from 50°S to 50°N.
fig. S4. Spatial distribution of winter CEs with CHL and NO_3 anomaly localized within their perimeter.
fig. S5. Spatial distribution of winter ACEs exhibiting strong positive and negative expressions of the first and second REOFs for satellite CHL (Fig. 2A).
fig. S6. Nitrate change from OFAM ACEs with their third principal component lower than 1 SD.
fig. S7. Evolution of a South Indian Ocean ACE in the OFAM.
fig. S8. Spatial distribution of CHL and NO_3 anomaly localized within the perimeter of ACEs during winter based on the third principal component of their REOF decomposition (see Fig. 2).
table S1. Mean relative difference between surface CHL in ACEs and surface CHL in CEs in the subtropical gyres during winter.
table S2. Spatial statistical parameters of the relative difference between surface CHL in ACEs and surface CHL in CEs in the subtropical gyres during winter.

REFERENCES AND NOTES

1. C. R. McClain, S. R. Signorini, J. R. Christian, Subtropical gyre variability observed by ocean color satellites. *Deep Sea Res. Pt. II* **51**, 281–301 (2004).
2. S. C. Doney, The ocean's productive deserts. *Nature* **389**, 905–906 (1997).
3. S. Emerson, P. Quay, D. Karl, C. Winn, L. Tupas, M. Landry, Experimental determination of the organic carbon flux from open ocean surface waters. *Nature* **389**, 951–954 (1997).
4. S. C. Doney, Oceanography: Plankton in a warmer world. *Nature* **444**, 695–696 (2006).
5. D. J. McGillicuddy Jr., Mechanisms of physical biological biogeochemical interaction at the oceanic mesoscale. *Annu. Rev. Mar. Sci.* **8**, 125–159 (2016).
6. A. Mahadevan, Ocean science: Eddy effects on biogeochemistry. *Nature* **506**, 168–169 (2014).
7. P. G. Falkowski, D. Ziemann, Z. Kolber, P. K. Bienfang, Role of eddy pumping in enhancing primary production in the ocean. *Nature* **352**, 55–58 (1991).
8. A. Waite, P. A. Thompson, S. Pesant, M. Feng, L. E. Beckley, C. M. Domingues, D. Gaughan, C. E. Hanson, C. M. Holl, T. Koslow, M. Meuleners, J. P. Montoya, T. Moore, B. A. Muhling, H. Paterson, S. Rennie, J. Strzelecki, L. Twomey, The Leeuwin Current and its eddies: An introductory overview. *Deep Sea Res. Pt. II* **54**, 789–796 (2007).
9. J. E. Greenwood, M. Feng, A. M. Waite, A one dimensional simulation of biological production in two contrasting mesoscale eddies in the south eastern Indian Ocean. *Deep Sea Res. Pt. II* **54**, 1029–1044 (2007).
10. P. Gaube, D. B. Chelton, P. G. Strutton, M. J. Behrenfeld, Satellite observations of chlorophyll, phytoplankton biomass, and Ekman pumping in nonlinear mesoscale eddies. *J. Geophys. Res. Oceans* **118**, 6349–6370 (2013).
11. L. Stramma, H. W. Bange, R. Czeschel, A. Lorenzo, M. Frank, On the role of mesoscale ed dies for the biological productivity and biogeochemistry in the eastern tropical Pacific Ocean off Peru. *Biogeosciences* **10**, 7293–7306 (2013).
12. D. B. Chelton, P. Gaube, M. G. Schlax, J. J. Early, R. M. Samelson, The influence of nonlinear mesoscale eddies on near surface oceanic chlorophyll. *Science* **334**, 328–332 (2011).
13. D. J. McGillicuddy Jr., L. A. Anderson, N. R. Bates, T. Bibby, K. O. Buesseler, C. A. Carlson, C. S. Davis, C. Ewart, P. G. Falkowski, S. A. Goldthwait, D. A. Hansell, W. J. Jenkins, R. Johnson, V. K. Kosnyrev, J. R. Ledwell, Q. P. Li, D. A. Siegel, D. K. Steinberg, Eddy/wind interac tions stimulate extraordinary mid ocean plankton blooms. *Science* **316**, 1021–1026 (2007).
14. P. Gaube, D. J. McGillicuddy Jr., D. B. Chelton, M. J. Behrenfeld, P. G. Strutton, Regional variations in the influence of mesoscale eddies on near surface chlorophyll. *J. Geophys. Res. Oceans* **119**, 8195–8220 (2014).
15. F. Dufois, N. J. Hardman Mountford, J. Greenwood, A. J. Richardson, M. Feng, S. Herbette, R. Matear, Impact of eddies on surface chlorophyll in the South Indian Ocean. *J. Geophys. Res. Oceans* **119**, 8061–8077 (2014).
16. D. B. Chelton, M. G. Schlax, R. M. Samelson, Global observations of nonlinear mesoscale eddies. *Prog. Oceanogr.* **91**, 167–216 (2011).
17. P. R. Oke, D. A. Griffin, A. Schiller, R. J. Matear, R. Fiedler, J. Mansbridge, A. Lenton, M. Cahill, M. A. Chamberlain, K. Ridgway, Evaluation of a near global eddy resolving ocean model. *Geosci. Model Dev.* **6**, 591–615 (2013).
18. S. Kouketsu, H. Tomita, E. Oka, S. Hosoda, T. Kobayashi, K. Sato, The role of meso scale eddies in mixed layer deepening and mode water formation in the western North Pacific. *J. Oceanogr.* **68**, 63–77 (2012).
19. D. A. Siegel, S. C. Doney, J. A. Yoder, The North Atlantic spring phytoplankton bloom and Sverdrup's critical depth hypothesis. *Science* **296**, 730–733 (2002).
20. S. Dutkiewicz, M. Follows, J. Marshall, W. W. Gregg, Interannual variability of phytoplankton abundances in the North Atlantic. *Deep Sea Res. Pt. II* **48**, 2323–2344 (2001).
21. S. Neuer, R. Davenport, T. Freudenthal, G. Wefer, O. Llinás, M. J. Rueda, D. K. Steinberg, D. M. Karl, Differences in the biological carbon pump at three subtropical ocean sites. *Geophys. Res. Lett.* **29**, 32 1–32 4 (2002).
22. P. G. Falkowski, Evolution of the nitrogen cycle and its influence on the biological seques tration of CO_2 in the ocean. *Nature* **387**, 272–275 (1997).
23. R. J. Matear, M. A. Chamberlain, C. Sun, M. Feng, Climate change projection for the western tropical Pacific Ocean using a high resolution ocean model: Implications for tuna fisheries. *Deep Sea Res. Pt. II* **113**, 22–46 (2015).
24. D. McGillicuddy Jr., L. A. Anderson, S. C. Doney, M. Maltrud, Eddy driven sources and sinks of nutrients in the upper ocean: Results from a 0.1° resolution model of the North Atlantic. *Global Biogeochem. Cycles* **17**, 1035 (2003).
25. W. J. Jenkins, Nitrate flux into the euphotic zone near Bermuda. *Nature* **331**, 521–523 (1988).
26. S. Emerson, S. Mecking, J. Abell, The biological pump in the subtropical North Pacific Ocean: Nutrient sources, Redfield ratios, and recent changes. *Global Biogeochem. Cycles* **15**, 535–554 (2001).
27. D. Chen, L. M. Rothstein, A. J. Busalacchi, A hybrid vertical mixing scheme and its application to tropical ocean models. *J. Phys. Oceanogr.* **24**, 2156–2179 (1994).
28. I. Halo, B. Backeberg, P. Penven, I. Ansorge, C. Reason, J. E. Ullgren, Eddy properties in the Mozambique Channel: A comparison between observations and two numerical ocean cir culation models. *Deep Sea Res. Pt. II* **100**, 38–53 (2014).

Acknowledgments: The Argo data were collected and made freely available by the International Argo Program and the national programs that contribute to it (www.argo.ucsd.edu, http://argo.jcommops.org). The Argo Program is part of the Global Ocean Observing System. We thank the NASA Ocean Biology for providing the SeaWiFS ocean color data, the National Oceanic and Atmospheric Administration World Ocean Atlas 2009 for the nitrate data, and P. Penven for providing an eddy tracking tool. **Funding:** Financial support for this study was provided by the Commonwealth Scientific and Industrial Research Organisation through the Oceans and Atmosphere flagship and the Office of the Chief Executive. **Author contributions:** All authors contributed to the design of the study. R.M. performed the model simulation. F.D. performed the analysis and prepared the manuscript. All authors commented on and edited the manuscript. **Competing interests:** The authors declare that they have no competing interests. **Data and materials availability:** All data needed to evaluate the conclusions in the paper are present in the paper and/or the Supplementary Materials. Additional data related to this paper may be requested from the authors.

Submitted 10 February 2016
Accepted 14 April 2016
Published 20 May 2016
10.1126/sciadv.1600282

Citation: F. Dufois, N. J. Hardman Mountford, J. Greenwood, A. J. Richardson, M. Feng, R. J. Matear, Anticyclonic eddies are more productive than cyclonic eddies in subtropical gyres because of winter mixing. *Sci. Adv.* **2**, e1600282 (2016).

Anticyclonic eddies are more productive than cyclonic eddies in subtropical gyres because of winter mixing

François Dufois, Nick J. Hardman-Mountford, Jim Greenwood, Anthony J. Richardson, Ming Feng and Richard J. Matear

Sci Adv **2** (5), e1600282.
DOI: 10.1126/sciadv.1600282